PHYSICAL REVIEW D **79,** 112012 (2009)

Study of the process $e^+e^- \to \mu^+\mu^-$ in the energy region $\sqrt{s} = 980$, 1040–1380 MeV

M. N. Achasov,* V. M. Aulchenko, K. I. Beloborodov, A. V. Berdyugin, A. G. Bogdanchikov, A. D. Bukin, D. A. Bukin, T. V. Dimova, V. P. Druzhinin, V. B. Golubev, I. A. Koop, A. A. Korol, S. V. Koshuba, A. P. Lysenko, E. V. Pakhtusova, E. A. Perevedentsev, S. I. Serednyakov, Yu. M. Shatunov, Z. K. Silagadze, A. N. Skrinsky, Yu. A. Tikhonov, and A. V. Vasiljev

Budker Institute of Nuclear Physics, Siberian Branch of the Russian Academy of Sciences, 11 Lavrentyev, Novosibirsk 630090, Russia
Novosibirsk State University, Novosibirsk 630090, Russia

(Received 5 October 2008; published 24 June 2009)

The cross section of the process $e^+e^- \to \mu^+\mu^-$ was measured in the spherical neutral detector experiment at the VEPP-2M e^+e^- collider in the energy region $\sqrt{s} = 980$, 1040–1380 MeV. The event numbers of the process $e^+e^- \to \mu^+\mu^-$ were normalized to the integrated luminosity measured using $e^+e^- \to e^+e^-$ and $e^+e^- \to \gamma\gamma$ processes. The ratio of the measured cross section to the theoretically predicted value is $1.006 \pm 0.007 \pm 0.016$ and $1.005 \pm 0.007 \pm 0.018$ in the first and second case, respectively. Using results of the measurements, the electromagnetic running coupling constant α in the energy region $\sqrt{s} = 1040$–1380 MeV was obtained $\langle 1/\alpha \rangle = 134.1 \pm 0.5 \pm 1.2$ and this is in agreement with theoretical expectation.

DOI: 10.1103/PhysRevD.79.112012 PACS numbers: 13.66.De, 12.20.Fv, 13.66.Jn, 14.60.Ef

I. INTRODUCTION

The process $e^+e^- \to \mu^+\mu^-$ is the simplest process in the electroweak theory and at the same time it constitutes an important tool in the high energy physics. It plays a fundamental role for studies of the electromagnetic and weak interactions, and electromagnetic properties of hadrons. This process was used for quantum electrodynamics (QED) tests, in electroweak interference studies, in leptonic width measurements of the $I^GJ^{PC} = 0^-1^{--}$ vector mesons and the Z boson, and for the study of the running electromagnetic coupling constant $\alpha(s)$.

The lowest order Feynman diagram of the process $e^+e^- \to \mu^+\mu^-$ in the energy region $\sqrt{s} < 2000$ MeV is shown in the Fig. 1(a). In Fig. 1(b) the diagram of vacuum polarization containing virtual lepton and quark pairs is also shown. These virtual pairs effectively shield a full charge that leads to energy dependence of the electromagnetic coupling constant

$$\alpha(s) = \frac{\alpha(0)}{1 - \Pi(s)}, \tag{1}$$

where $\Pi(s)$ is the vacuum polarization. The vacuum polarization with leptonic pairs is computed theoretically in the QED framework, while the hadronic vacuum polarization is computed by using dispersion integral and the experimental $e^+e^- \to$ hadrons cross section.

The process $e^+e^- \to \mu^+\mu^-$ in the energy region $\sqrt{s} <$ 2000 MeV was studied earlier in several experiments. In Refs. [1–3] the tests of QED with low statistics were reported. In Ref. [4] the cross section of the $e^+e^- \to \mu^+\mu^-$ process was measured with accuracy of about 1% in the energy region $\sqrt{s} = 370$–520 MeV. The studies of the $\phi \to \mu^+\mu^-$ decay were reported in Refs. [5,6].

For the studies of the process $e^+e^- \to \mu^+\mu^-$ with the spherical neutral detector (SND) the most convenient energy region is $\sqrt{s} > 980$ MeV. Here the value of the $e^+e^- \to \mu^+\mu^-$ process cross section is equal or higher than the cross section of the main background process $e^+e^- \to \pi^+\pi^-$ and the muons are detected with a SND muon system. The SND results of the $\phi \to \mu^+\mu^-$ decay study were published in Refs. [7,8]. In this work the results of the $e^+e^- \to \mu^+\mu^-$ process analysis in the energy region $\sqrt{s} = 980$, 1040–1380 MeV, based on the integrated luminosity 6.4 pb^{-1} is presented.

II. EXPERIMENT

The SND detector [9] operated from 1995 to 2000 at the VEPP-2M [10] collider in the energy range $\sqrt{s}$ from 360 to 1400 MeV. The detector contains several subsystems. The tracking system includes two cylindrical drift chambers.

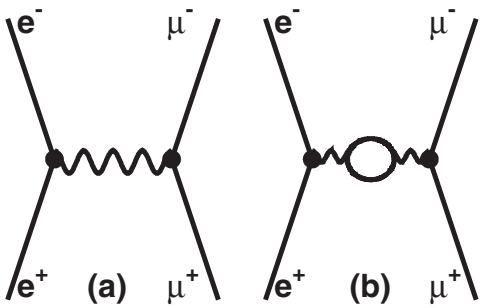

FIG. 1. Feynman diagrams of the process $e^+e^- \to \mu^+\mu^-$: (a) diagram in the lowest order; (b) vacuum polarization diagram, the loops are due to fermion pairs—electrons, muons, τ leptons, and quarks.

*achasov@inp.nsk.su

The three-layer spherical electromagnetic calorimeter is based on NaI(Tl) crystals. The muon and veto system consists of plastic scintillation counters and two layers of streamer tubes. The calorimeter energy and angular resolutions depend on the photon energy as $\sigma_E/E(\%) = 4.2\%/\sqrt[4]{E(\mathrm{GeV})}$ and $\sigma_{\phi,\theta} = 0.82^\circ/\sqrt{E(\mathrm{GeV})} \oplus 0.63^\circ$. The tracking system angular resolutions are about 0.5° and 2° for azimuthal and polar angles, respectively.

III. DATA ANALYSIS

The cross section of the $e^+e^- \to \mu^+\mu^-$ process was measured in the following way.

(1) The collinear events $e^+e^- \to \mu^+\mu^-$, $e^+e^- \to e^+e^-$, and $e^+e^- \to \gamma\gamma$ were selected.

(2) The $e^+e^- \to e^+e^-$ and $e^+e^- \to \gamma\gamma$ events were used for integrated luminosity determination:

$$\mathrm{IL} = \frac{N}{\sigma(s)\varepsilon(s)}, \tag{2}$$

where N, $\sigma(s)$, and $\varepsilon(s)$ are event number, cross section, and detection efficiency for the process $e^+e^- \to e^+e^-$ or $e^+e^- \to \gamma\gamma$.

(3) The cross section of the process $e^+e^- \to \mu^+\mu^-$ was obtained as

$$\sigma_{\mu\mu}(s) = \frac{N}{\mathrm{IL}\varepsilon(s)\delta_{\mathrm{rad}}(s)}. \tag{3}$$

Here N is the selected events number of the process $e^+e^- \to \mu^+\mu^-$, IL is integrated luminosity, $\varepsilon(s)$ is the detection efficiency, and $\delta_{\mathrm{rad}}(s)$ is the radiative correction which takes into account the emission of photons by the initial and final particles [11,12].

The detection efficiency was obtained from Monte Carlo (MC) simulation [9,13]. In order to obtain the detection efficiency of the $e^+e^- \to \mu^+\mu^-$ process, the MC events generator based on the formula obtained in Ref. [14] was used. MC simulation of the processes $e^+e^- \to e^+e^-$ and $e^+e^- \to \gamma\gamma$ was based on the formulas obtained in Refs. [15,16]. The simulation of the process $e^+e^- \to e^+e^-$ was performed with the cut $30^\circ < \theta_{e^\pm} < 150^\circ$ on the polar angles of the final electron and positron. The cross section under these conditions was computed by using BHWIDE [17] code with accuracy 0.5%.

The Feynman diagrams of the processes $e^+e^- \to e^+e^-$ and $e^+e^- \to \gamma\gamma$ in the lowest order are shown in Figs. 2 and 3. The process $e^+e^- \to e^+e^-$ also contains the contribution from the vacuum polarization due to leptons and hadrons virtual pairs (Fig. 4), while the process $e^+e^- \to \gamma\gamma$ does not have such contributions. Hence to obtain the deviation of $\alpha(s)$ from $\alpha(0)$, the process $e^+e^- \to \gamma\gamma$ is preferable for normalization.

In this work the cross section of the process $e^+e^- \to \mu^+\mu^-$ was obtained based on integrated luminosities measured by using both $e^+e^- \to e^+e^-$ (IL_{ee}) and $e^+e^- \to \gamma\gamma$ ($\mathrm{IL}_{\gamma\gamma}$) processes. The cross section of the process $e^+e^- \to e^+e^-$ in the angular region $30^\circ < \theta_{e^\pm} < 150^\circ$ was measured by using integrated luminosity $\mathrm{IL}_{\gamma\gamma}$

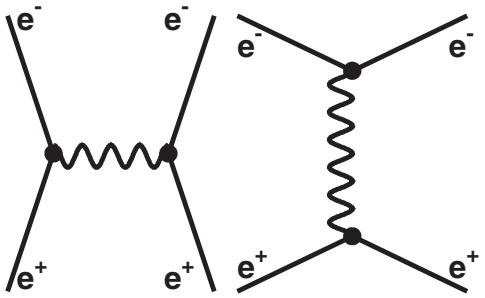

FIG. 2. The Feynman diagrams of the $e^+e^- \to e^+e^-$ process in lowest order.

$$\sigma_{e^+e^-(\gamma)} = \frac{N_{e^+e^-}}{\mathrm{IL}_{\gamma\gamma}\varepsilon_{e^+e^-}}, \tag{4}$$

where $N_{e^+e^-}$ and $\varepsilon_{e^+e^-}$ are the event number and detection efficiency for the process $e^+e^- \to e^+e^-$.

A. Selection criteria

During the experimental runs, first-level trigger selects events of various types: events with charged particles and events containing neutral particles only. In the first case, the trigger selected events with one or more tracks in the tracking system and with two clusters in the calorimeter with the spatial angle between the clusters more than 100°. The threshold on the energy deposition in each cluster was equal to 25 MeV. The threshold on the total energy deposition in the calorimeter was set equal to 160 MeV. In the second case, the events without tracks in the tracking system and with veto signal of the muon system and with total energy deposition more than 250 MeV were selected. During processing of the experimental data, the event reconstruction is performed [9,18]. The reconstructed particles were sorted in the decreasing order of their energy deposition in the calorimeter. Further the first two particles were considered. They were numbered in the following way: in odd events the particle which has the higher energy deposition in the calorimeter was named the first one and in

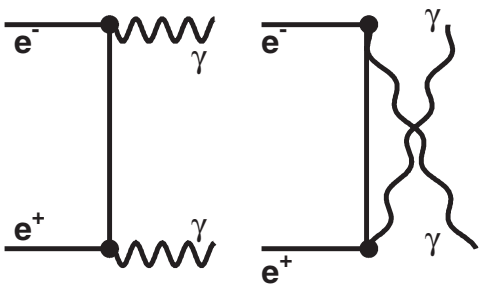

FIG. 3. The Feynman diagram of the $e^+e^- \to \gamma\gamma$ process in lowest order.

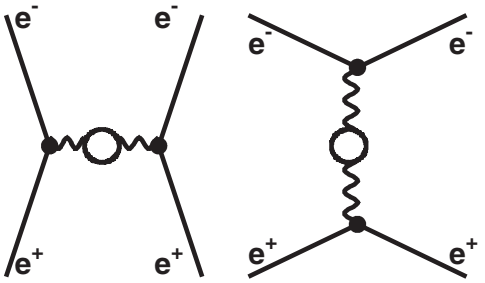

FIG. 4. The Feynman diagrams of the process $e^+e^- \to e^+e^-$ with vacuum polarization due to virtual fermion pairs (electrons, muons, τ leptons, and quarks).

the even events the first particle was the particle with lower energy deposition.

The $e^+e^- \to \gamma\gamma$ process events were selected by using the following selection criteria (below subscripts 1 and 2 denote the first and second particles, respectively):

(i) $N_{\rm cha} = 0$ and $N_{\rm neu} \geq 2$, where $N_{\rm cha}$, $N_{\rm neu}$ are the numbers of charged and neutral particles (photons). Extra photons in the $e^+e^- \to \gamma\gamma$ events can appear because of overlap with the beam background, due to electromagnetic showers splitting or to the higher order process $e^+e^- \to \gamma\gamma\gamma$.
(ii) $55^\circ < \theta_1 < 125^\circ$, where θ is the particle polar angle
(iii) $|\Delta\theta| = |180^\circ - (\theta_1 + \theta_2)| < 20^\circ$.
(iv) $|\Delta\phi| = |180^\circ - |\phi_1 - \phi_2|| < 5^\circ$, where ϕ is the particle azimuthal angle.
(v) $E_{1,2}/E_0 > 0.7$, where E_i is the ith photon ($i = 1, 2$) energy deposition and E_0 is the beam energy.

The events of the processes $e^+e^- \to e^+e^-$ and $e^+e^- \to \mu^+\mu^-$ were selected in the following way:

(i) $N_{\rm cha} = 2$. The events can contain neutral particles due to overlap with the beam background or due to electromagnetic showers splitting.
(ii) $|z_{1,2}| < 10$ cm and $r_{1,2} < 1$ cm, where z is the coordinate of the charged particle production point along the beam axis (the longitudinal size of the interaction region depends on beam energy and varies from 2 to 3 cm) and r is the distance between the charged particle track and the beam axis in the $r - \phi$ plane.
(iii) $55^\circ < \theta_1 < 125^\circ$.
(iv) $|\Delta\phi| < 10^\circ$ and $|\Delta\theta| < 10^\circ$.
(v) The region of $240^\circ < \phi_{1,2} < 300^\circ$ was excluded, because this sector of the ϕ angle was not covered with the muon system.
(vi) $r_1 < 0.1$ cm or $r_2 < 0.1$ cm. This cut strongly suppressed the contribution of cosmic muons in the events selected as $e^+e^- \to \mu^+\mu^-$.

The last two selection criteria were not applied in the measurement of the $e^+e^- \to e^+e^-$ process cross section.

Finally the $e^+e^- \to e^+e^-$ events were selected by using cuts on the particles energy depositions $E_{1,2}/E_0 > 0.7$. The selection of the $e^+e^- \to \mu^+\mu^-$ events was done by using the following cuts $E_{1,2} > 50$ MeV and $E_{1,2}/E_0 < 0.7$. In addition, each particle was required to fire the scintillation counters of the muon system.

B. Background determination

The selection criteria described above allow for extracting the events of processes $e^+e^- \to e^+e^-$ and $e^+e^- \to \gamma\gamma$ without any significant background admixture. The data selected as events of the $e^+e^- \to \mu^+\mu^-$ process contain about 45% of the cosmic muon background. In order to extract the $e^+e^- \to \mu^+\mu^-$ events number $n_{\mu\mu}$, the distribution over the coordinate $z = (z_1 + z_2)/2$ (Fig. 5) was fitted by the sum

$$G(z) \times n_{\mu\mu} + C(z) \times (n - n_{\mu\mu}), \tag{5}$$

where n is the total number of selected events, $G(z)$ is the Gaussian distribution for $e^+e^- \to \mu^+\mu^-$ events with peak at $z = 0$ cm, $C(z)$ is the uniform distribution for cosmic background events. The $C(z)$ distribution was obtained by using data collected in special runs without beams in collider. The $G(z)$ distribution was obtained in each energy point by using $e^+e^- \to e^+e^-$ events. The systematic uncertainty of $n_{\mu\mu}$ determination was estimated by using distributions for the $e^+e^- \to \pi^+\pi^-$ and K^+K^- events instead of z distribution for the $e^+e^- \to e^+e^-$ events in Eq. (5) in the role of $G(z)$. The difference in $n_{\mu\mu}$ values obtained by fitting with various $G(z)$ was found to be 0.5% and this value was taken as systematic error due to the cosmic background subtraction.

Besides cosmic background, the selected data contain events of the collinear $e^+e^- \to e^+e^-$ and $e^+e^- \to \pi^+\pi^-$ processes (the expected background from the $e^+e^- \to K^+K^-$, $e^+e^- \to 3\pi$, 4π, K_SK_L processes is less than 0.05%). The expected event number $N_{\pi\pi}$ from the $e^+e^- \to \pi^+\pi^-$ process is less than 1.1% of the $e^+e^- \to \mu^+\mu^-$

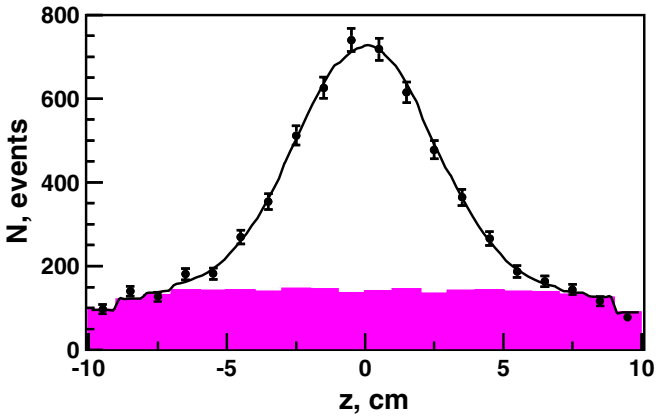

FIG. 5 (color online). The distribution of the z coordinate of the charged particles production point in events selected as $e^+e^- \to \mu^+\mu^-$ at the energy $\sqrt{s} = 1370$ MeV. Dots—all events; dashed distribution—cosmic background events; and curve—the fit by sum of distributions of beam and cosmic events.

event number and was estimated in the following way:

$$N_{\pi\pi} = \sigma_{\pi\pi}(s)\varepsilon_{\pi\pi}(s)\mathrm{IL}, \quad (6)$$

where $\sigma_{\pi\pi}(s)$ is the cross section of the $e^+e^- \to \pi^+\pi^-$ process measured by OLYA and CMD-2 detectors [19,20], IL is the integrated luminosity, $\varepsilon_{\pi\pi}(s)$ is the detection probability for the background process obtained from the simulation under the selection criteria described above. The source of error in the $N_{\pi\pi}$ determination is an inaccurate simulation of the muon system efficiency. To estimate this error the $e^+e^- \to \pi^+\pi^-$ events were selected at the energy point $\sqrt{s} = 980$ MeV (below the $e^+e^- \to K^+K^-$ reaction threshold) by using additional cuts:

(i) $r_{1,2} < 0.1$ cm (for the cosmic background suppression).
(ii) $E_1^{II} < 50$ MeV and $E_1^{III} < 50$ MeV, where E_1^{II} and E_1^{III} are the first particle energy depositions in the second and third calorimeter layers, respectively, (for $e^+e^- \to \mu^+\mu^-$ and cosmic background suppression).
(iii) The muon system was not fired by the first particle and no requirements for the second particle.

Under these conditions the $e^+e^- \to e^+e^-$ process background is negligible, the cosmic background was subtracted using z distribution. The following value was obtained:

$$\delta_{\pi\pi} = \left(\frac{n/N}{m/M}\right)^2 = 0.4 \pm 0.4 \quad (7)$$

Here N and M are the number of experimental and simulated events of the process $e^+e^- \to \pi^+\pi^-$ selected under described criteria, while n and m are the event numbers in experiment and simulation in which the muon system was fired by the second particle. The accuracy of $\delta_{\pi\pi}$ is equal to its value, due to the low statistics.

In the energy region above the $e^+e^- \to K^+K^-$ reaction threshold up to $\sqrt{s} = 1100$ MeV the $\delta_{\pi\pi}$ correction can be obtained by using cuts on the dE/dx ionization energy losses in the drift chamber for the charged kaons background rejection. In particular at $\sqrt{s} = 1100$ MeV it was found that $\delta_{\pi\pi} = 0.8 \pm 0.5$, and this agrees with the estimation presented above.

In order to check the systematic uncertainty due to inaccuracy of the $N_{\pi\pi}$ subtraction, the probability $\varepsilon_{\pi\pi}(s)$ in all energy points was multiplied by $\delta_{\pi\pi} = 0.4$. After this the measured $e^+e^- \to \mu^+\mu^-$ process cross section has changed by less than 0.7%. This value was taken as the systematic error due to the $e^+e^- \to \pi^+\pi^-$ background subtraction.

The expected value of the $e^+e^- \to e^+e^-$ events background is about 0.2% of the $e^+e^- \to \mu^+\mu^-$ events number. The systematic error due to subtraction of this background was found to be negligible.

C. Detection efficiency

Uncertainties in the simulation of the distributions over some selection parameters lead to the inaccuracy in detection efficiency determination. In order to estimate this inaccuracy the experimental and simulated spectra were studied and compared using additional cuts. These cuts were selected so that they were uncorrelated with the studied parameter and provided the distribution over this parameters without additional background admixture.

The muon system firing is the main cut for the extraction of the $e^+e^- \to \mu^+\mu^-$ process events. The comparison of the simulated and experimental probabilities of the muon system firing was done by using the following additional cuts:

(i) $r_{1,2} < 0.1$ cm (for the cosmic muon background suppression).
(ii) The muon system was fired by the first particle and no requirements for the second particle.
(iii) $30 < E_{1,2}^{I} < 55$ MeV, $45 < E_{1,2}^{II} < 80$ MeV and $55 < E_{1,2}^{III} < 90$ MeV, where E_i^j is the ith particle energy deposition in the jth calorimeter layer (for $e^+e^- \to \pi^+\pi^-$ and K^+K^- background rejection).

Then the following parameter was calculated:

$$\delta_{sc} = \left(\frac{n/N}{m/M}\right)^2, \quad (8)$$

where N, M are selected numbers of experimental and simulated events and n, m are the event numbers in experiment and simulation in which the muon system was fired by the second particle also. The cosmic background was subtracted using z distribution. The coefficient δ_{sc} is equal to 1.15 ± 0.028 at $\sqrt{s} = 980$ MeV and decreases to 1.004 ± 0.002 at $\sqrt{s} = 1380$ MeV. The detection efficiency of the process $e^+e^- \to \mu^+\mu^-$ at various energy points was multiplied by correction coefficient at this point.

The energy deposition spectra of the muons in calorimeter is shown in Fig. 6. The experimental and simulated distributions are in good agreement. No significant system-

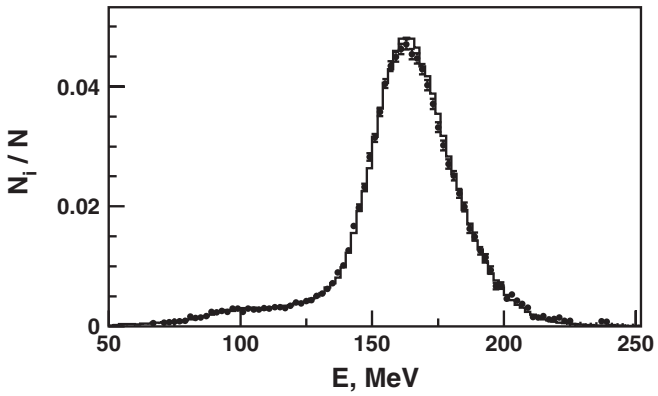

FIG. 6. Energy deposition spectra for the muons in experiment (dots) and simulation (histogram).

atics were found due to the cuts on the energy deposition in the $e^+e^- \to \mu^+\mu^-$ process.

In the tracking system the particle track can be lost due to reconstruction inefficiency. The probabilities to find both tracks were determined by using experimental data themselves. It was found to be $\varepsilon_{ee} \simeq 0.982 \pm 0.001$ and $\varepsilon_{\mu\mu} \simeq 0.983 \pm 0.001$ for processes $e^+e^- \to e^+e^-$ and $e^+e^- \to \mu^+\mu^-$ respectively. In simulations, these values do not actually differ from unity. Thus, if the event numbers of the process $e^+e^- \to \mu^+\mu^-$ were normalized by the integrated luminosity IL_{ee}, the systematic errors due to track reconstruction are actually reduced. When the events of the $e^+e^- \to e^+e^-$ and $e^+e^- \to \mu^+\mu^-$ processes were normalized by the luminosity $\mathrm{IL}_{\gamma\gamma}$, the detection efficiencies were multiplied by coefficients ε_{ee} and $\varepsilon_{\mu\mu}$.

The cuts on the $r_{1,2}$ also lead to some inaccuracy of the detection efficiency. To obtain the corresponding correction factor to the detection efficiency of the process $e^+e^- \to \mu^+\mu^-$, the events of the process $e^+e^- \to \pi^+\pi^-$ were used because in the region $r_{1,2} > 0.1$ cm the cosmic background dominates and for its rejection the muon system veto is required, which excludes the $e^+e^- \to \mu^+\mu^-$ events also. At the energies under study, muons and pions velocities are about the same and the drift chamber response on their passage is just the same. In order to exclude the events of the $e^+e^- \to K^+K^-$ process, the correction coefficient was obtained by using data collected at the energy $\sqrt{s} = 980$ MeV. MC simulation shows that the ratio of event numbers with $r_{1,2} < 0.1$ and $r_{1,2} > 0.1$ is the same for $e^+e^- \to \mu^+\mu^-$ and $e^+e^- \to \pi^+\pi^-$ processes and does not depend on energy.

As a result, the detection efficiency of the process $e^+e^- \to \mu^+\mu^-$ was multiplied by the correction coefficient $\delta_r^{\mu\mu} = 0.982 \pm 0.005$. The error is due to uncertainty of the cosmic muons background subtraction and it was added to the systematic error of the detection efficiency.

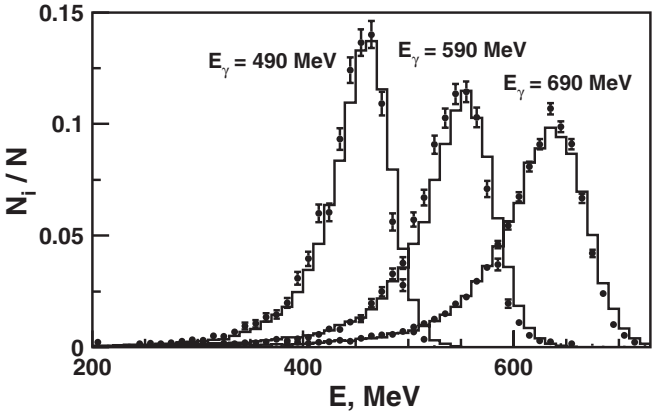

FIG. 8. Energy deposition spectra for photons with energies of 490, 590, and 690 MeV in experiment (dots) and simulation (histogram).

Analogously the correction coefficient $\delta_r^{ee} = 0.993$ was used for the IL_{ee} measurement.

The energy deposition spectra in calorimeter for $e^{\pm}$ and γ are shown in Fig. 7 and 8. The experimental and simulated distributions are in good agreement. The detection efficiency correction factor values due to the cuts $E_{1,2}/E_0 > 0.7$ are usually less than 1%, but in some energy points it reaches about 3% and was taken into account for luminosity determination. These corrections are the same for both $e^+e^- \to e^+e^-$ and $e^+e^- \to \gamma\gamma$ processes—the average value of the correction factors ratio is equal to 1.001 ± 0.001.

The $\Delta\phi$ and $\Delta\theta$ distributions of the $e^+e^- \to e^+e^-$, $\gamma\gamma$, and $\mu^+\mu^-$ events are shown in Figs. 9–14. The apparent shifts in the $\Delta\theta$ data distribution can be attributed to an offset in the z coordinate of the interaction vertex. As a measure of the systematic uncertainty due to the $\Delta\theta$ cut, the following parameter was used:

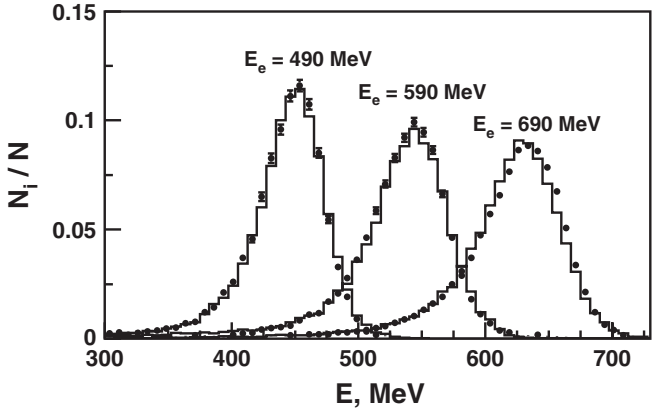

FIG. 7. Energy deposition spectra for electrons with energies of 490, 590, and 690 MeV in experiment (dots) and simulation (histogram).

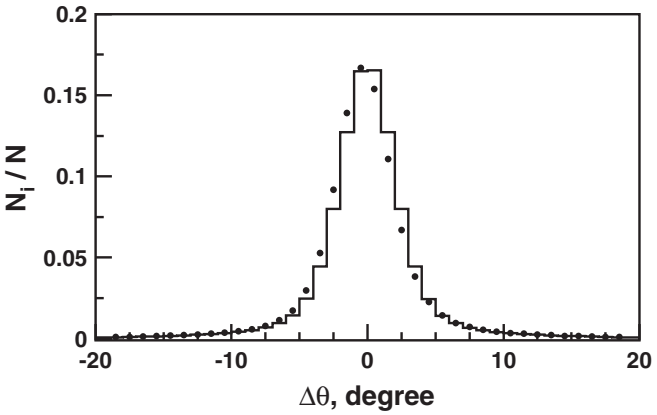

FIG. 9. The $\Delta\theta$ distribution of the $e^+e^- \to e^+e^-$ events. Dots—experiment; histogram—simulation.

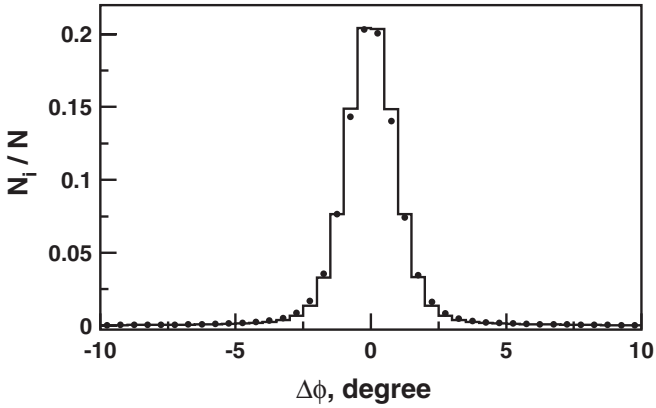

FIG. 10. The $\Delta\phi$ distribution of the $e^+e^- \to e^+e^-$ events. Dots—experiment; histogram—simulation.

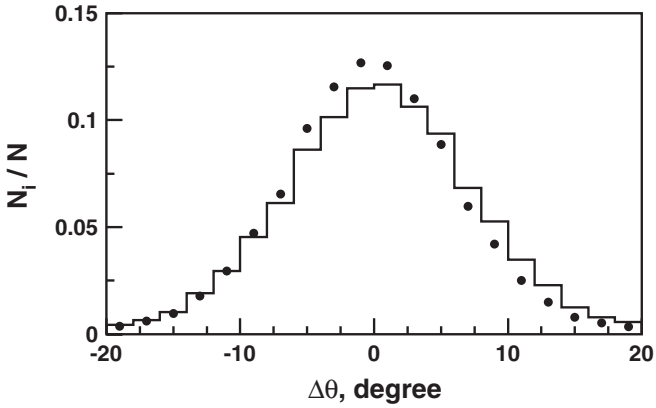

FIG. 11. The $\Delta\theta$ distribution of the $e^+e^- \to \gamma\gamma$ events. Dots—experiment; histogram—simulation.

$$\delta^x_{\Delta\theta} = \frac{n_x(|\Delta\theta| < 10^\circ)}{N_x(|\Delta\theta| < 20^\circ)} \Big/ \frac{m_x(|\Delta\theta| < 10^\circ)}{M_x(|\Delta\theta| < 20^\circ)}, \quad x = \mu\mu(ee). \tag{9}$$

Here $n_x(|\Delta\theta| < 10^\circ)$ and $m_x(|\Delta\theta| < 10^\circ)$ are the numbers

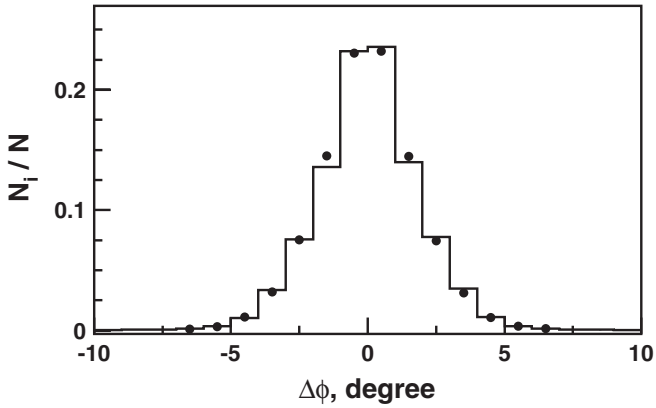

FIG. 12. The $\Delta\phi$ distribution of the $e^+e^- \to \gamma\gamma$ events. Dots—experiment; histogram—simulation.

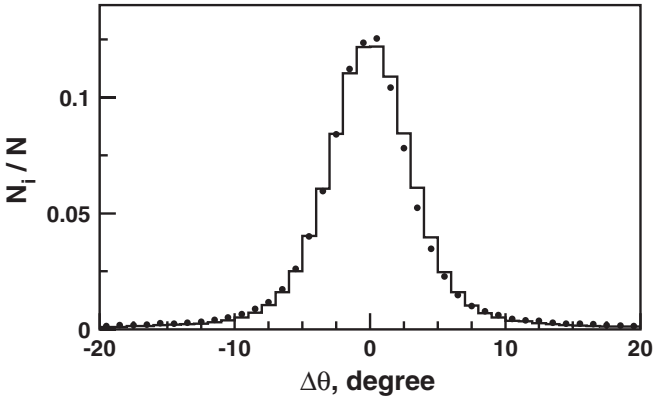

FIG. 13. The $\Delta\theta$ distribution of the $e^+e^- \to \mu^+\mu^-$ events. Dots—experiment; histogram—simulation.

of experimental and simulated events selected under the condition $|\Delta\theta| < 10^\circ$, while $N_x(|\Delta\theta| < 20^\circ)$ and $M_x(|\Delta\theta| < 20^\circ)$ are the numbers of experimental and simulated events with $|\Delta\theta| < 20^\circ$. The average values of $\delta^{ee}_{\Delta\theta}$ and $\delta^{\mu\mu}_{\Delta\theta}$ are equal to 0.999, and have systematic spread of 0.002 and 0.007, respectively. The $\delta^{ee}_{\Delta\theta}$ and $\delta^{\mu\mu}_{\Delta\theta}$ were used as correction coefficients to the detection efficiencies of corresponding processes.

The variation of the $\Delta\theta$ cut by 5° for the $e^+e^- \to \gamma\gamma$ process leads to the variation of the integrated luminosity $\mathrm{IL}_{\gamma\gamma}$ by 0.9%. This value was added to the systematic uncertainty of the integrated luminosity measurement. Systematic error due to the $\Delta\phi$ cut was found to be negligible for all processes.

The polar angle distributions for the $e^+e^- \to e^+e^-$, $e^+e^- \to \mu^+\mu^-$, and $e^+e^- \to \gamma\gamma$ processes are shown in Figs. 15–17. The ratios of these θ distributions are shown in Fig. 18 and 19. The experimental and simulated distributions are in good agreement. The shapes of the distributions do not depend on energy and for all processes is almost the same for the angles $\theta \approx 80^\circ$. Using all collected data, the following coefficients were obtained:

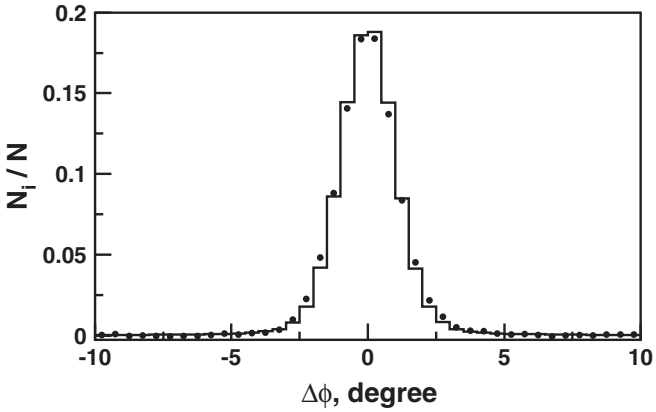

FIG. 14. The $\Delta\phi$ distribution of the $e^+e^- \to \mu^+\mu^-$ events. Dots—experiment; histogram—simulation.

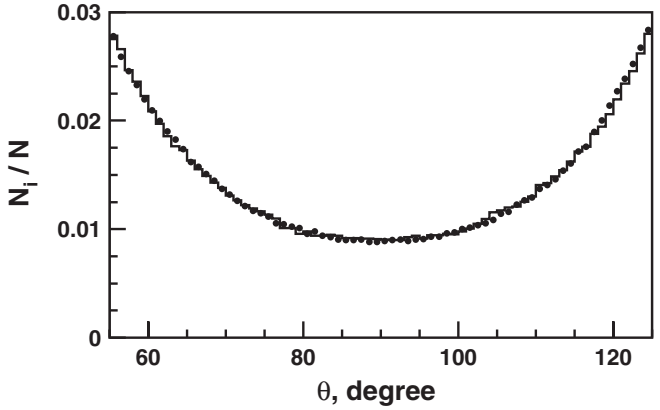

FIG. 15. The θ angle distribution of the $e^+e^- \to e^+e^-$ events. Dots—experiment; histogram—simulation.

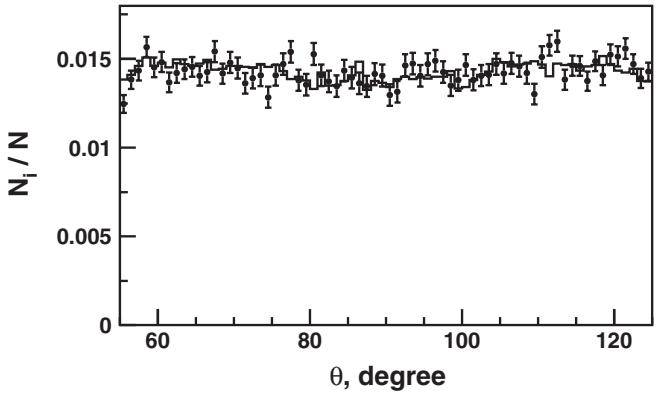

FIG. 16. The θ angle distribution of the $e^+e^- \to \mu^+\mu^-$ events. Dots—experiment; histogram—simulation.

$$\delta_\theta^x = \frac{n_x}{N_x} \Big/ \frac{m_x}{M_x}, \qquad x = \mu\mu(ee, \gamma\gamma), \tag{10}$$

where N_x and M_x are the experimental and simulated event numbers in the angular range $55° < \theta < 125°$, while n_x and m_x are the experimental and simulated event numbers

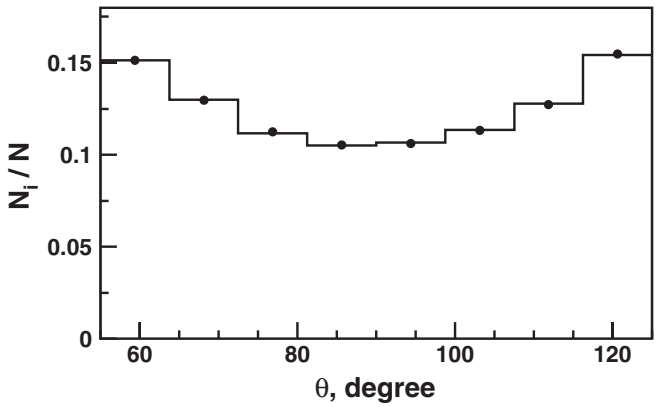

FIG. 17. The θ angle distribution of the $e^+e^- \to \gamma\gamma$ events. Dots—experiment; histogram—simulation.

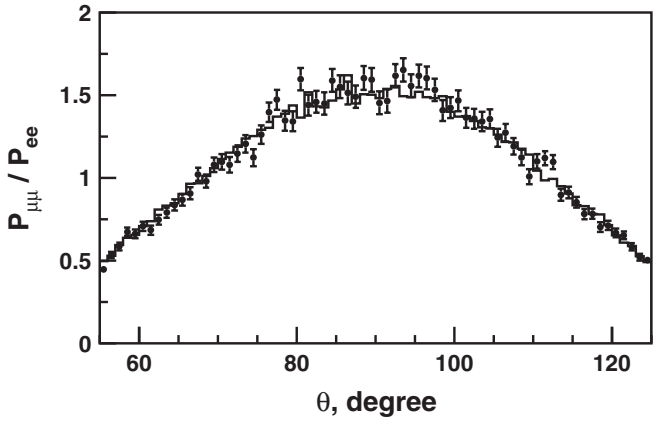

FIG. 18. The ratio of the θ distributions of the $e^+e^- \to \mu^+\mu^-$ and $e^+e^- \to e^+e^-$ events. Dots—experiment; histogram—simulation.

in the angular range $80° < \theta < 100°$. In order to estimate the systematic inaccuracy due to the cut on the θ angle, the following ratio was used:

$$\delta_\theta = \frac{\delta_\theta^x}{\delta_\theta^y}, \qquad x = \mu\mu(ee), \qquad y = ee(\gamma\gamma) \tag{11}$$

This ratio was used as the correction factor to the cross section. For the process $e^+e^- \to \mu^+\mu^-$, the δ_θ is equal to 1.015 ± 0.010 and 1.02 ± 0.01 when it is normalized on the $e^+e^- \to e^+e^-$ and $e^+e^- \to \gamma\gamma$ processes, respectively. For the process $e^+e^- \to e^+e^-$ normalized on the $e^+e^- \to \gamma\gamma$ events, $\delta_\theta = 0.995 \pm 0.005$. The δ_θ error was included in the total systematic error.

The first-level trigger selection criteria for the $e^+e^- \to \gamma\gamma$ process events included the absence of tracks in the short drift chamber (nearest to the beam-pipe). This leads to the trigger dead time due to the overlap of a background track. The trigger inefficiency of about 5% was hardware

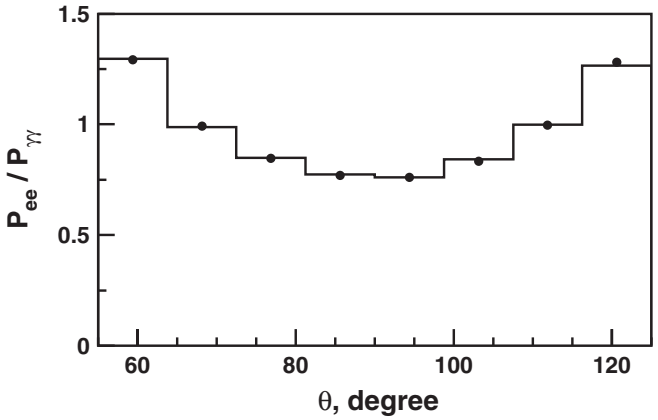

FIG. 19. The ratio of the θ distributions of the $e^+e^- \to e^+e^-$ and $e^+e^- \to \gamma\gamma$ events. Dots—experiment; histogram—simulation.

measured during the data taking and was taken into account in the analysis.

In $e^+e^- \to \gamma\gamma$ process events, the charged particle can appear due to the photon conversion on the detector material before the tracking system. As a measure of the systematic inaccuracy associated to this effect, the difference from unity of the following quantity was used:

$$\delta_{\rm con} = \left(1 - \frac{n}{3N}\right) \Big/ \left(1 - \frac{m}{3M}\right), \qquad (12)$$

where N and M are the photon numbers in the experiment and simulation; n and m are the photons in the experiment and simulation which had a track in the second drift chamber. The probability to find a track was divided by 3 which is the ratio of amounts of matter between the drift chambers and before the tracking system. The result $\delta_{\rm con} = 0.998 \pm 0.002$ shows that the difference between photon conversion probabilities in the experiment and simulation does not contribute much in the error of the measurements.

D. Measured cross sections

The cross sections of the process $e^+e^- \to \mu^+\mu^-$ and $e^+e^- \to e^+e^-$ are listed in Table I. The total systematic error of the cross section $\sigma^{ee}_{\mu\mu}$ (obtained by using IL_{ee} luminosity) determination is

$$\sigma_{\rm sys} = \sigma_{\rm eff} \oplus \sigma_{\rm bkg} \oplus \sigma_{\rm rad} \oplus \sigma_{\rm IL} = 1.6\%.$$

Here $\sigma_{\rm eff}$ is the systematic error of the detection efficiency determination, $\sigma_{\rm bkg}$ is the systematic error due to background subtraction, $\sigma_{\rm IL}$ is the systematic error of integrated luminosity determination due to inaccuracy of the $e^+e^- \to e^+e^-$ cross section calculation and $\sigma_{\rm rad}$ is the uncertainty of the radiative correction calculation. The magnitudes of various contributions to the total systematic error are shown in Table II.

The total systematic error of the cross section $\sigma^{\gamma\gamma}_{\mu\mu}$ (obtained by using $\mathrm{IL}_{\gamma\gamma}$ luminosity) determination is

$$\sigma_{\rm sys} = \sigma_{\rm eff} \oplus \sigma_{\rm bkg} \oplus \sigma_{\rm rad} \oplus \sigma_{\rm IL} = 1.8\%.$$

Here $\sigma_{\rm IL}$ is the systematic error of the integrated luminosity determination which includes the inaccuracy of the $e^+e^- \to \gamma\gamma$ cross section calculation and the $\Delta\theta$ angle measurement error. The magnitudes of various contributions to the total systematic error are shown in Table II.

The total systematic error of the $\sigma_{ee(\gamma)}$ cross section determination (of the $e^+e^- \to e^+e^-$ process in the angular region $30^\circ < \theta_{e^\pm} < 150^\circ$) is

$$\sigma_{\rm sys} = \sigma_{\rm eff} \oplus \sigma_{\rm IL} = 1.1\%.$$

The magnitudes of various contributions are also listed in Table II.

TABLE I. The main results of this work. $\sigma^{\gamma\gamma}_{\mu\mu}$ is the $e^+e^- \to \mu^+\mu^-$ cross section obtained by using luminosity $\mathrm{IL}_{\gamma\gamma}$, $\sigma_{ee(\gamma)}$ is the cross section of the process $e^+e^- \to e^+e^-$ in the angular range $30^\circ < \theta_{e^\pm} < 150^\circ$. Only uncorrelated errors are shown. The correlated systematic error $\sigma_{\rm sys}$ is 1.8% for $\sigma^{\gamma\gamma}_{\mu\mu}$ and 1.1% for $\sigma_{ee(\gamma)}$.

$\sqrt{s}$ (MeV)	$\sigma^{\gamma\gamma}_{\mu\mu}$, nb	$\sigma_{ee(\gamma)}$, nb
980	96.3 ± 5.6	2898 ± 34
1040	83.6 ± 4.4	2539 ± 44
1050	82.3 ± 4.0	2553 ± 39
1060	84.1 ± 3.7	2512 ± 44
1070	80.6 ± 3.5	2441 ± 36
1080	82.7 ± 3.7	2351 ± 41
1090	72.8 ± 3.0	2316 ± 35
1100	77.8 ± 3.8	2371 ± 26
1110	69.7 ± 2.9	2288 ± 36
1120	71.6 ± 3.7	2195 ± 37
1130	71.6 ± 2.7	2170 ± 31
1140	67.6 ± 3.4	2170 ± 36
1150	70.7 ± 4.0	2121 ± 38
1160	73.0 ± 3.2	2091 ± 31
1180	66.8 ± 3.1	2073 ± 31
1190	61.8 ± 2.4	1936 ± 25
1200	66.8 ± 4.4	1961 ± 21
1210	65.6 ± 2.7	1872 ± 26
1220	58.5 ± 2.5	1853 ± 26
1230	67.6 ± 3.2	1858 ± 26
1240	59.3 ± 2.4	1794 ± 24
1250	58.8 ± 2.1	1798 ± 22
1260	56.7 ± 2.3	1718 ± 23
1270	57.9 ± 1.8	1728 ± 21
1280	53.5 ± 1.7	1664 ± 20
1290	51.1 ± 1.5	1668 ± 19
1300	54.4 ± 1.6	1638 ± 18
1310	52.7 ± 2.0	1608 ± 21
1320	48.5 ± 1.9	1556 ± 19
1330	52.9 ± 1.8	1538 ± 18
1340	49.8 ± 1.7	1586 ± 20
1350	49.5 ± 2.1	1507 ± 18
1360	50.9 ± 1.7	1541 ± 19
1370	45.0 ± 1.9	1476 ± 18
1380	48.4 ± 1.5	1459 ± 15

IV. DISCUSSION

The measured cross section of the process $e^+e^- \to e^+e^-$ (Table I) was fitted with the following expression:

$$\sigma_{ee(\gamma)} = C_{\rm fit} \times \frac{C_{\rm BHWIDE}}{s},$$

where $C_{\rm BHWIDE}$ is the coefficient calculated by using BHWIDE code [17]. The accuracy of calculation is about 0.5%. $C_{\rm fit}$ is the ratio of the measured cross section to theoretically expected (calculated) value and it was a free parameter of the fit. As a result, it was obtained that (Fig. 20)

TABLE II. Various contributions to the systematic error of the cross sections determination. $\sigma_{\rm sys}$ is the total systematic error.

The Source of the Error	Contribution to $\sigma^{ee}_{\mu\mu}$	Contribution to $\sigma^{\gamma\gamma}_{\mu\mu}$	Contribution to $\sigma_{ee(\gamma)}$
The θ Distribution	1.0%	1.0%	0.5%
The r Distribution	0.5%	0.5%	...
$\sigma_{\rm eff}$	1.1%	1.1%	0.5%
The Cosmic Background Subtraction	0.5%	0.5%	...
The Background from the $e^+e^- \to \pi^+\pi^-$ Process Subtraction	0.7%	0.7%	...
$\sigma_{\rm bkg}$	0.9%	0.9%	...
$\sigma_{\rm rad}$	0.5%	0.5%	...
The $\Delta\theta$ Distribution in the $e^+e^- \to \gamma\gamma$ Process	...	0.9%	0.9%
Calculation of the $e^+e^- \to e^+e^-$ Process Cross Section	0.5%	...	...
Calculation of the $e^+e^- \to \gamma\gamma$ Process Cross Section	...	0.5%	0.5%
$\sigma_{\rm IL}$	0.5%	1.0%	1.0%
$\sigma_{\rm sys}$	1.6%	1.8%	1.1%

$$C_{\rm fit} = 0.999 \pm 0.002 \pm 0.011.$$

The measured value of the $e^+e^- \to e^+e^-$ cross section is in good agreement with the calculation.

The $e^+e^- \to \mu^+\mu^-$ cross section was fitted with the following formula:

$$\sigma_{\mu\mu} = \frac{4\pi}{3s}\frac{\alpha(0)^2}{|1-\Pi(s)|^2}\frac{\beta}{4}(6-2\beta^2)\times C_{\rm fit}, \qquad \beta = \sqrt{1-\frac{4m_\mu^2}{s}}. \tag{13}$$

From the fit of the $\sigma^{ee}_{\mu\mu}$ cross section, it was found that

$$C_{\rm fit} = 1.006 \pm 0.007 \pm 0.016,$$

which agrees well with theoretical predictions.

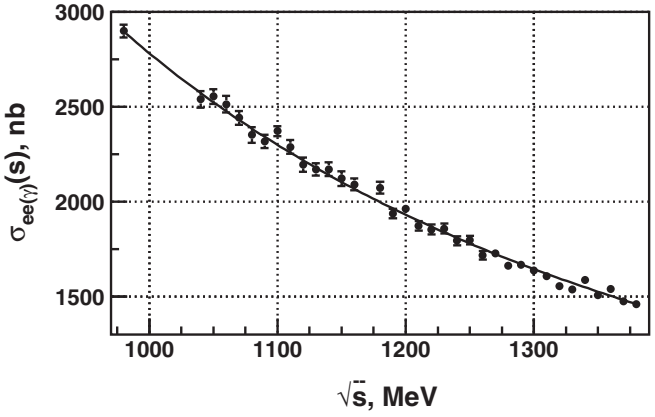

FIG. 20. The $e^+e^- \to e^+e^-$ cross section in the angular range $30° < \theta_{e^\pm} < 150°$. Dots are the SND data obtained in this work; the curve is the result of the fit ($\chi^2/N_{\rm d.o.f.} = 48.1/34$).

In the similar energy region $\sqrt{s} = 370$–520 MeV, the $e^+e^- \to \mu^+\mu^-$ process cross section was measured by the CMD-2 detector with accuracy about 1.5% [4]. In this experiment the integrated luminosity was obtained by using $e^+e^- \to e^+e^-$ process. The $C_{\rm fit}$ for this data was found to be $C_{\rm fit} = 0.980 \pm 0.013 \pm 0.007$. In order to compare the SND and CMD-2 results, the following ratio was examined:

$$C^{\rm SND}_{\rm fit}/C^{\rm CMD-2}_{\rm fit} = 1.027 \pm 0.015 \pm 0.018.$$

The difference between the SND and CMD-2 results (Fig. 21) is 1.2 standard deviations.

From the fit of the $\sigma^{\gamma\gamma}_{\mu\mu}$ cross section (Table I, Fig. 22) it was found that

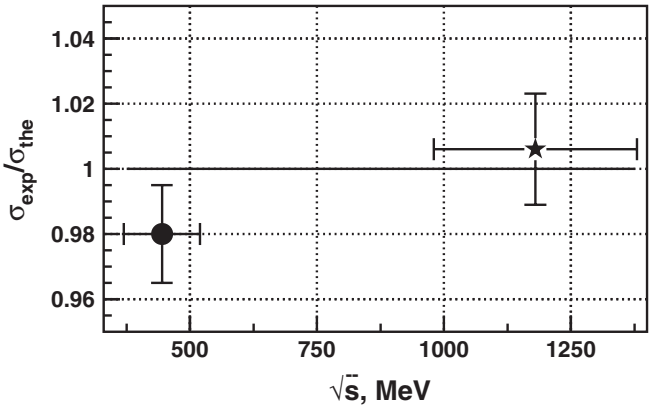

FIG. 21. The ratio $\sigma_{\rm exp}/\sigma_{\rm the}$ of the $e^+e^- \to \mu^+\mu^-$ cross section measured by SND ($\star$, this work) and CMD-2 (●, [4]) to theoretical value. The horizontal bars show the energy region $\sqrt{s}$ in which the cross section was measured.

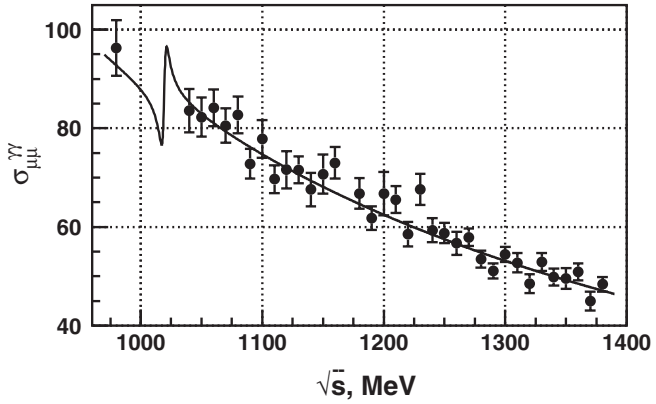

FIG. 22. The $e^+e^- \to \mu^+\mu^-$ cross section obtained by using $IL_{\gamma\gamma}$. Dots are the SND data obtained in this work; the curve is the result of the fit ($\chi^2/N_{\text{d.o.f.}} = 37.2/34$).

$$C_{\text{fit}} = 1.005 \pm 0.007 \pm 0.018.$$

If the fit is performed with the average value $\langle 1/\alpha \rangle$ as a free parameter, that is, by using the function to fit data

$$\sigma_{\mu\mu} = \frac{4\pi}{3s}\frac{\beta}{4}(6 - 2\beta^2) \times \left[\frac{1}{\langle 1/\alpha \rangle}\right]^2, \qquad (14)$$

then

$$\langle 1/\alpha \rangle = 134.1 \pm 0.5 \pm 1.2.$$

This value of $\langle 1/\alpha \rangle$ agrees with the expected one, and the difference from $\alpha(0)$ is 2.3 standard deviations. The obtained value of $\langle 1/\alpha \rangle$ together with other results in the timelike region is shown in Fig. 23. The black markers denote the measurements with normalization independent from vacuum polarization diagrams. The results of this work is the only measurement of such a type at the low energy ($\simeq 1$ GeV) region.

A new e^+e^- collider VEPP-2000 for the energy region $\sqrt{s}$ up to 2 GeV with the SND and CMD-2 detectors have now being launching. In the future experiments the $e^+e^- \to \mu^+\mu^-$ cross section can be measured with accuracy better then 1% and it will be a good test of the theory.

V. CONCLUSION

The cross section of the process $e^+e^- \to \mu^+\mu^-$ was measured in the SND experiment at the VEPP-2M e^+e^- collider in the energy region $\sqrt{s} = 980$, 1040–1380 MeV using integrated luminosity obtained from the $e^+e^- \to e^+e^-$ and $e^+e^- \to \gamma\gamma$ processes. The accuracy of the cross section determination is about 1.6% and 1.8%, respectively. The ratio of the measured cross section to the theoretically predicted value is $1.006 \pm 0.007 \pm 0.016$ and $1.005 \pm 0.007 \pm 0.018$ in the first and second case, respectively. Using results of the measurements, the electromagnetic coupling constant α was obtained in the energy region $\sqrt{s} = 1040$–1380 MeV: $\langle 1/\alpha \rangle = 134.1 \pm 0.5 \pm 1.2$. The cross section of the process $e^+e^- \to e^+e^-$ was also measured in the angular region $30° < \theta_{e^\pm} < 150°$ with systematic accuracy 1.1%. The ratio of the measured cross section to the theoretically calculated one is $0.999 \pm 0.002 \pm 0.011$.

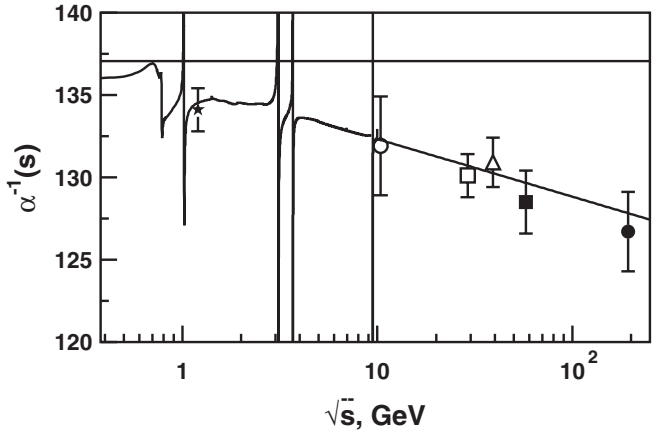

FIG. 23. The $\alpha(s)^{-1}$ values obtained by using different experiment results. The SND ($\star$, this work), TOPAZ (■, [21]), and OPAL (●, [22]) results are presented. The dots from review [23] obtained using results of experiments at DORIS (○), PEP (□), and PETRA (△) colliders are presented also. Horizontal line shows the $\alpha(0)^{-1}$ value; curve is theoretical calculation of $\alpha(s)^{-1}$.

ACKNOWLEDGMENTS

The work is supported in part by RF Presidential Grant for Scientific School NSh-5655.2008.2, and RFBR 08-02-00328-a, 08-02-00660-a, 08-02-00634-a, 06-02-16192-a, and 06-02-16294-a.

[1] B. Borgia *et al.*, Lett. Nuovo Cimento Soc. Ital. Fis. **3**, 115 (1972).
[2] V. E. Balakin *et al.*, Phys. Lett. **37B**, 435 (1971).
[3] V. Alles-Borelli *et al.*, Phys. Lett. **59B**, 201 (1975).
[4] R. R. Akhmetshin *et al.*, Pis'ma Zh. Eksp. Teor. Fiz. **84**, 491 (2006) [JETP Lett. **84**, 413 (2006)].
[5] L. M. Kurdadze *et al.*, Yad. Fiz. **35**, 352 (1982) [Sov. J. Nucl. Phys. **35**, 201 (1982)].
[6] F. Ambrosino *et al.*, Phys. Lett. B **608**, 199 (2005).
[7] M. N. Achasov *et al.*, Phys. Lett. B **456**, 304 (1999).
[8] M. N. Achasov *et al.*, Phys. Rev. Lett. **86**, 1698 (2001).
[9] M. N. Achasov *et al.*, Nucl. Instrum. Methods Phys. Res., Sect. A **449**, 125 (2000).
[10] A. N. Skrinsky, in *Proceedings of Workshop on Physics*

and Detectors for DAΦNE, Frascati Physics Series Vol. 4 (INFN Laboratori Nazionzli di Frascati, Frascati, Italy, 1995), p. 3.
[11] E. A. Kuraev and V. S. Fadin, Yad. Fiz. **41**, 733 (1985) [Sov. J. Nucl. Phys. **41**, 466 (1985)].
[12] Yu. M. Bystritskiy *et al.*, Phys. Rev. D **72**, 114019 (2005).
[13] M. N. Achasov *et al.*, Zh. Eksp. Teor. Fiz. **128**, 1201 (2005).
[14] A. B. Arbuzov *et al.*, J. High Energy Phys. 10 (1997) 001.
[15] F. A. Berends and R. Kleiss, Nucl. Phys. **B228**, 537 (1983).
[16] F. A. Berends and R. Kleiss, Nucl. Phys. **B186**, 22 (1981).
[17] S. Jadach, W. Placzek, and B. F. L. Ward, Phys. Lett. B **390**, 298 (1997).
[18] M. N. Achasov *et al.*, Phys. Rev. D **63**, 072002 (2001).
[19] L. M. Barkov *et al.*, Nucl. Phys. **B256**, 365 (1985).
[20] V. M. Aulchenko *et al.*, Pis'ma Zh. Eksp. Teor. Fiz. **82**, 841 (2005) [JETP Lett. **82**, 743 (2005)].
[21] L. Levine *et al.*, Phys. Rev. Lett. **78**, 424 (1997).
[22] G. Abbiendi *et al.*, Eur. Phys. J. C **33**, 173 (2004).
[23] M. Kobel, in *The XVIII International Symposium on Lepton Photon Interactions*, edited by A. Roeck and A. Wagner (World Scientific, Hamburg, 1997).